Journal of Nuclear Materials 382 (2008) 197–202

Contents lists available at ScienceDirect

Journal of Nuclear Materials

journal homepage: www.elsevier.com/locate/jnucmat

Microstructural development in a model austenitic alloy following electron and ion irradiation

N. Sakaguchi [a], H. Kinoshita [a], S. Watanabe [a], Y. Sueishi [a], N. Akasaka [b], H. Takahashi [a,*]

[a] Center for Advanced Research of Energy Conversion Materials, Hokkaido University, Kita-ku, Kita-13, Nishi-8, Sapporo 060 8628, Japan
[b] Japan Atomic Energy Agency, O-Arai Research and Development Center, O-Arai, Ibaraki 311-1393, Japan

A B S T R A C T

In order to study the microstructural evolution of cascade and interaction between cascade and He, the irradiations were carried out using ion accelerator to introduce the cascade and a high resolution high voltage electron microscope (1250 kV) to irradiate with electrons and for *in situ* observation. A lot of small cascades were introduced by Ni^+-ion irradiation at room temperature, and due to following electron irradiation at higher temperature interstitial type dislocation loops were nucleated from the interstitials rich zone and grew. On the other hand the cascades transferred to SFTs during annealing above 623 K. When He atoms were previously implanted, He bubbles were formed at cascades. Also segregation of solutes and precipitates were induced at cascades during electron irradiation.

1. Introduction

The radiation-induced phenomenon are important for the materials exposed to energetic neutron irradiation circumstance such as fusion reactor, fast breeder reactor and light water reactors because the mechanical and chemical properties are influenced due to the irradiation introduced defects [1–3].

Thus the activities in this field have based not only on the academic understanding of intrinsic properties of these defects and their agglomerates but also on the practical concern that both physical and mechanical properties of metals and alloys.

Ion irradiation produces a clear separation between vacancies and interstitials, with a rich vacancy core in the damaged area and surrounding self-interstitials atoms [4].

The formation of stacking fault tetrahedral (SFT) as a defects have been confirmed in cascades in Cu by molecular dynamics (MD) simulations [5–7] and also by the direct observation in Cu, Ni and Au during 2 MeV electron irradiation [8] and the evolution of SFTs was deduced from the post-irradiation observations as well as from *in situ* dynamic observations [9]. The effects of cascade on structural evolution are mainly focused on void nucleation but the studies on segregation and/or precipitation induced during irradiation and the interaction with helium produced by (n, α) reaction [10–12] are little. The main purpose of this paper is to investigate the effects of cascade damage and its evolution under interaction with point defects and helium in an austenitic alloy by means of irradiations ion and electron.

After introducing cascade damage by ion irradiation, the evolution of cascade with solute and helium such as the radiation-induced segregation (RIS) around the cascade damage was observed during electron irradiation with a high resolution high voltage electron microscope.

2. Experimental procedures

A model alloy of high-purity Fe–15Cr–20Ni containing 0.5 wt%Si was used in this study. Composition of other impurities, such as carbon and phosphorus, was less than 0.001 wt%. The foils with about 200 nm in thickness for transmission electron microscopy (TEM) observation were prepared after cold rolling followed by solution treatment at 1323 K for 0.5 h and then air-cooled.

The specimens after electro-polishing were irradiated with 150 keV Ni^+ ions at 1.1×10^{16} ions/m^2/s (10^{-3} dpa/s) at room temperature up to 2.2×10^{17} ions/m^2 (0.02 dpa), where the mean depth of damage peak was about 20 nm from surface. No surface contamination was observed at the present ion irradiation condition. Then, electron irradiations were carried out using ultra high resolution high voltage electron microscope (1.25 MV HVEM, point resolution is 0.12 nm) at 623 K and 773 K. The electron irradiation damage rate and total dose were 5×10^{-4} dpa/s and 1.8 dpa, respectively. Helium ions were further implanted with 50 keV at room temperature to 2.6×10^{21}/m^2 (100 appm He at depth of 100 nm) after Ni^+ ion irradiation for a part of foils. The EDS analysis were also performed for the irradiated specimens by 200 kV FEG-TEM.

* Corresponding author. Tel.: +81 11 706 6767; fax: +81 11 757 3537.
E-mail address: takahash@ufml.caret.hokudai.ac.jp (H. Takahashi).

0022-3115/$ - see front matter © 2008 Elsevier B.V. All rights reserved.
doi:10.1016/j.jnucmat.2008.08.025

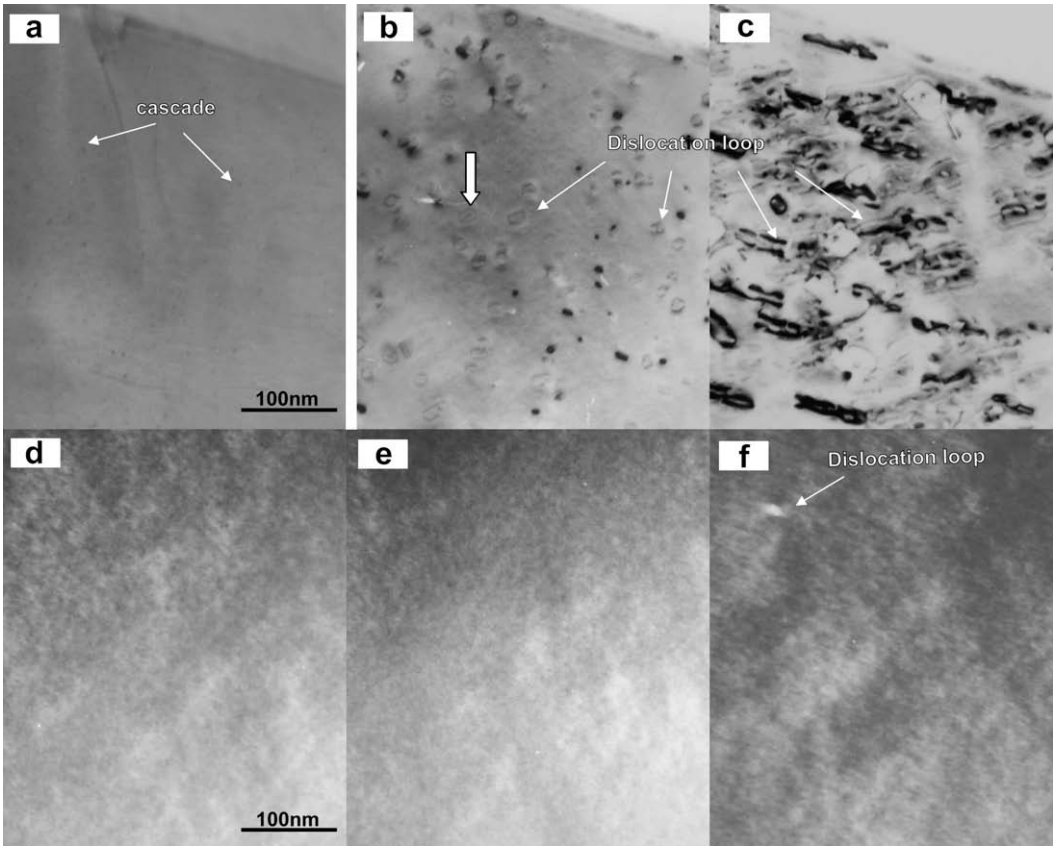

Fig. 1. Evolution of dislocation from cascade damage region (a) as-Ni^+-ion irradiation, (b) electron irradiation for 0.9 dpa, (c) 1.8 dpa, (d) only electron irradiation for 0 dpa, (e) 0.9 dpa, and (f) 1.8 dpa.

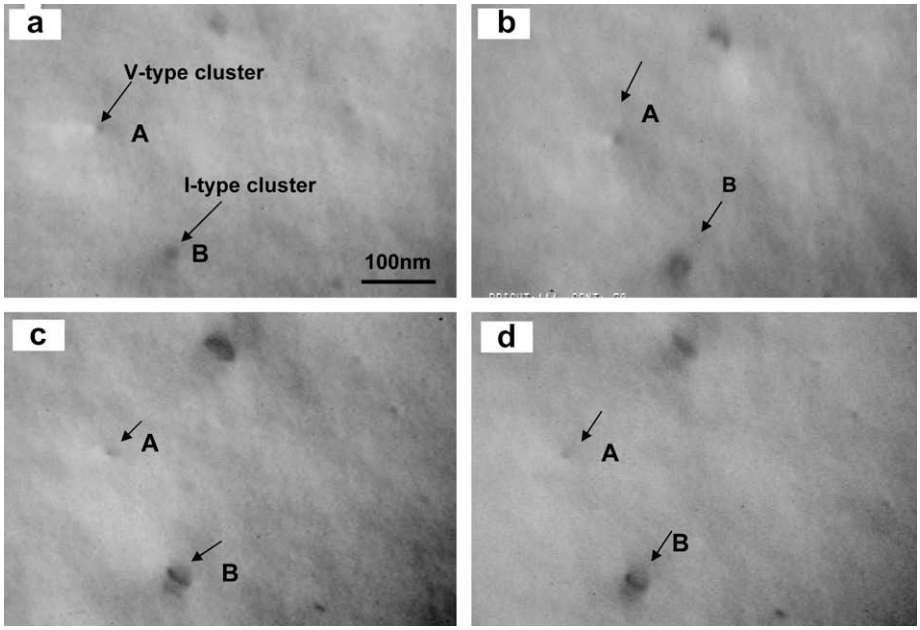

Fig. 2. Evolution of damage clusters introduced Ni^+-ion irradiation during electron irradiation at 623 K: (a) 0 dpa, (b) 0.3 dpa, (c) 0.6 dpa, and (d) 0.9 dpa.

3. Results and discussion

3.1. Cascade introduction and SFT formation

When foil specimens were electron irradiated at room temperature before and after ion irradiation, the evolution of microstructures showed different behavior depending on with and without pre-ion irradiation. Fig. 1(a)–(c) are microstructures of as-Ni^+-ion irradiation at room temperature and following electron irradiation at 623 K. As shown in Fig. 1(a), the cascade damage structure was observed as distribution of the dot-like contrast, and due to following electron irradiation in HVEM the cascades grew (Fig. 1(b)).

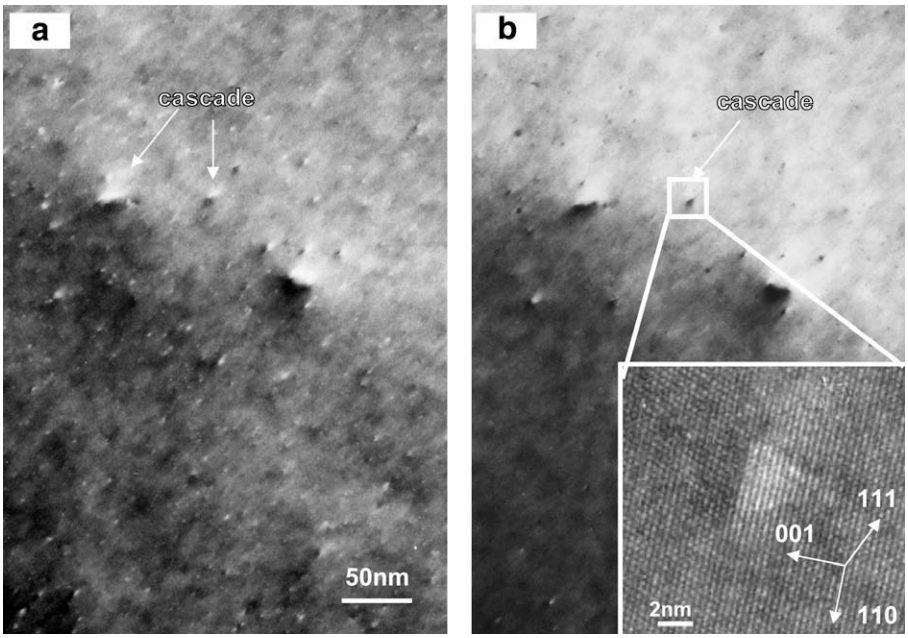

Fig. 3. Transfer of cascade to SFTs due to annealing: (a) as-Ni^{+} ion irradiation at R.T, (b) high resolution image of SFT formed during annealing at 623 K.

With further electron irradiation the formation and growth of dislocation loops as being observed in Fig. 1(c), which nucleated at cascade damage region, presumably interstitials rich zone formed outside of cascade [4], were observed. Furthermore other defects cluster was observed inside of grown dislocation loops as indicated by arrow. They might be vacancy cluster introduced in cascade since the specimen thickness was thin enough to neglect a superposition effect due to the projection imaging of both the defect clusters.

On the other hand, when the foil specimen was electron-irradiated without pre-ion irradiation, very few number of dislocation loops were formed even after high electron irradiation dose as shown in Fig. 1(d)–(f). This is suggested that interstitials rich clusters introduced in the process of cascade formation acts as preferential nucleation site of dislocation loops. On the other hand the dislocation loop nucleation is not easy in the case of only single electron irradiation because of no pre-existence of defect clusters (presumably interstitials) which assists dislocation loop nucleation and most of defects produced during electron irradiation diffused out from thin foil specimen surface.

In order to identify the nature of defects clusters introduced due to ion irradiation, the evolution of microstructures following electron irradiation electron irradiation was examined as *in situ* observation at 623 K. The results were shown in Fig. 2(a)–(c), where two types of defect clusters were observable, namely one of them shrunk (A) and other (B) continued to grow with further electron irradiation. At this irradiation temperature of 623 K, both of interstitials and vacancies introduced by electron irradiation can diffuse but the mobility of interstitials is very high comparing to vacancy. Namely when the interstitials with higher mobility were absorbed at interstitial loop, the loops grow and cascades consisted of vacancy rich cluster shrinks. These results suggest that the shrunk and the grown clusters under electron irradiation are corresponding to vacancy and interstitials type, respectively.

Fig. 3 shows the microstructures of the as-ion-irradiated and following annealing at 673 K to examine the stability of defect clusters introduced by Ni^{+} ion irradiation. Fig. 3(a) shows the as-ion irradiated cascade distribution and Fig. 3(b) shows structure with a high resolution lattice image after annealing at 673 K. It can be seen that the cascade transferred to SFT due to annealing,

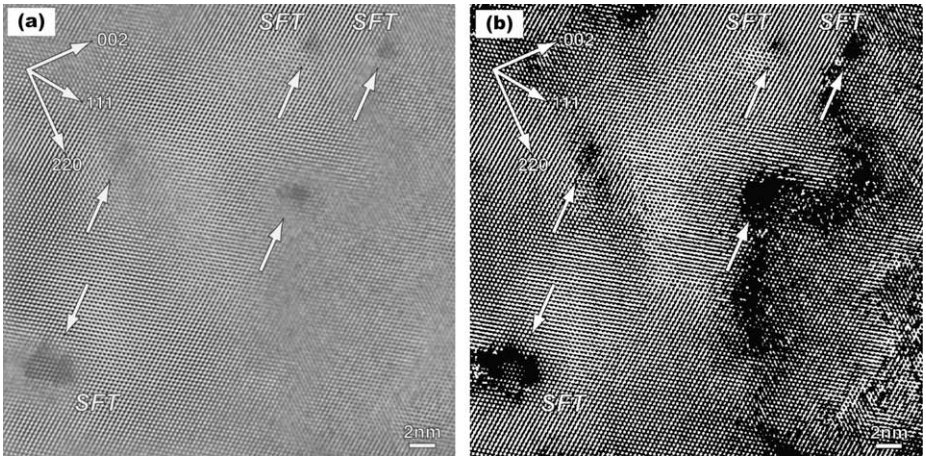

Fig. 4. (a) High resolution lattice image of SFTs and damaged ion path, (b) high contrast image of (a) higher contrast image of photo (a).

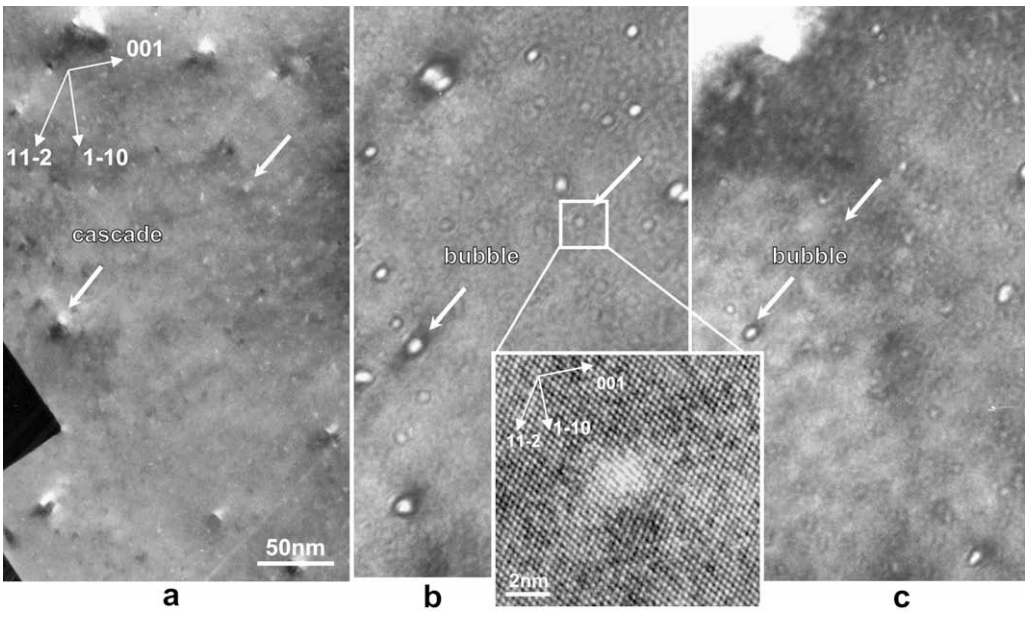

Fig. 5. He bubble formation during annealing at 673 K and following electron irradiation to 0.45 dpa after Ni^+ irradiation followed by He^+ ion implantation of 2.6×10^{21} ions/m^2: (a) as-Ni^+-ion and He irradiated to, (b) after annealing, (c) after electron irradiation.

which could be formed due to the cascade collapsed during annealing [13,14].

The more detailed images around SFT were observed with high resolution image and with higher contrast image. Fig. 4 (a) shows a high resolution lattice image observed (1 1 0) zone axis and (b) is the corresponding higher contrast image. Areas with darker contrast (indicated by arrows) in the lattice image were corresponding to SFTs with triangle sharp formed at cascades. Besides the lattice image the blurred image was recognized among SFTs, which distorted locally along a given direction. Fig. 4(b) shows the image of distorted zone emphasized by separating from non-distorted area, where the distorted areas were observed as higher dark contrast image. It is obviously from these structures recognized that some parts of SFTs were linked through the narrow distorted zone which correspond to the trucks caused by ions irradiation [15]. From the orientation relationship of these truck zones, the observed zones were along <1 1 0> or <1 1 2> on {1 1 1} plane. These results might be suggesting the trace of collision path of ions. Also dislocations were often observed around the trucks.

3.2. Effect of He on cascade evolution

It is well known that when stainless steels were neutron irradiated, gaseous He atoms were produced as a transmutation of (n, α)

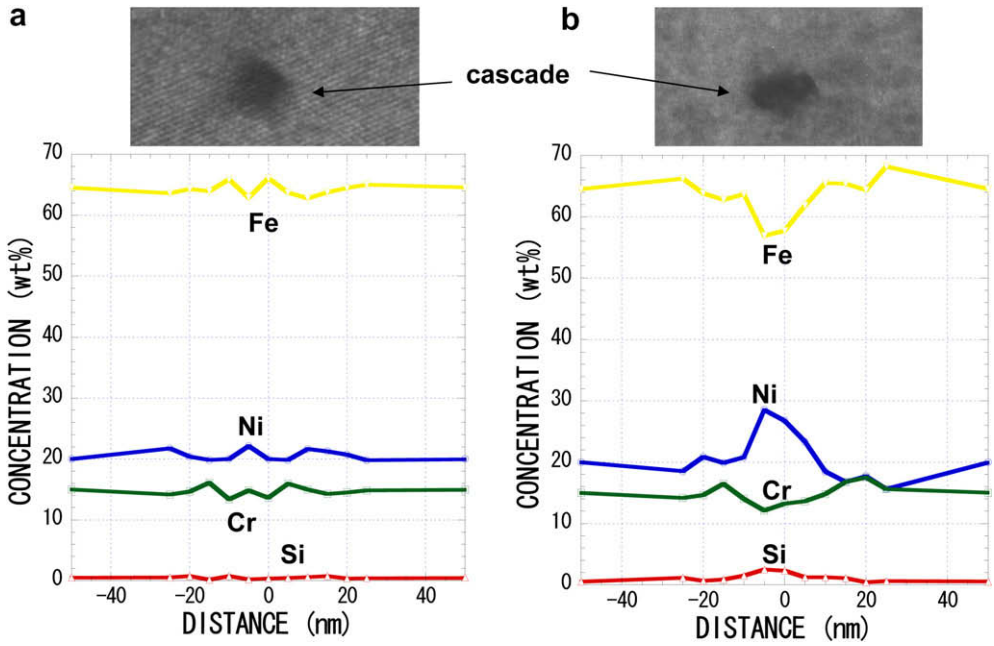

Fig. 6. Irradiation-induced solutes segregation at cascade: (a) microstructures of cascades after electron irradiation to 0.9 dpa at 723 K, (b) compositional analysis of solutes in matrix and cascade.

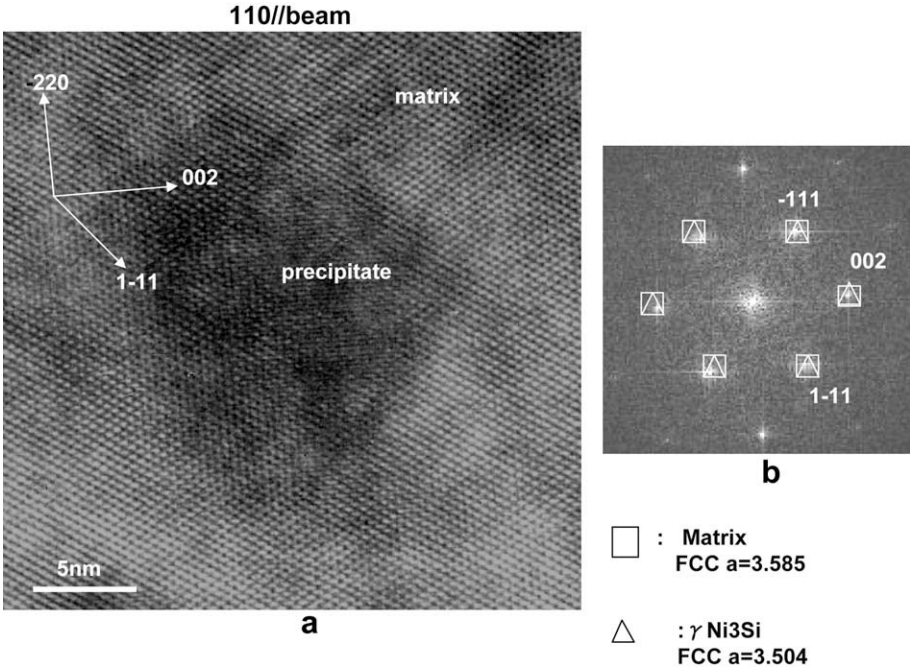

Fig. 7. Irradiation-induced precipitate after electron irradiation to 0.9 dpa at 723 K: (a) high resolution image of precipitate and matrix, and (b) FFT diffraction pattern from precipitate and matrix.

nuclei reaction [11], and He causes embrittlement and swelling in the materials. As cascade damage produces the vacancies rich zone [9], it is expected that the zone can act as sink site not only for point defects but also for He atoms. To study the effects of interaction between cascade and He atoms, the microstructural evolution of cascade after introducing cascades was observed as *in situ* experiments with ion irradiation followed by He^+ ion implantation.

Fig. 5 shows the microstructures of cascade after Ni^+ ion irradiation and He^+ implantation at room temperature, and He bubbles formed due to annealing at 673 K. This He bubble formation indicates that He atoms diffused into cascade with vacancy rich during annealing. The cascade region with bubbles was electron-irradiated at the same temperature of 673 K but obvious change of microstructure could not recognize. Therefore the cascade region filled by He would not act as effective sink site for point defects introduced by following irradiation.

3.3. RIS and RIP at cascade

Radiation-induced segregation of solutes would takes place at cascade damage region because the cascades are one of sink sites for point defects. Fig. 6 shows compositional profile before and after electron irradiation obtained by EDS analysis around cascade introduced after ion irradiation. The enrichment of Ni and Si and Cr depletion were recognized around cascade (see Fig. 6(a)) and the segregation increased due to following electron irradiation at 723 K as being observed in Fig. 6(b). The occurrence of segregation for the as-ion irradiated indicates that solutes preferentially diffuse toward cascade during ion and electron irradiations. The segregation accompanied with electron irradiation was mainly enhanced by general rule of size effect [16,17]. When local concentration of segregated solutes was increased to nucleate precipitate, the precipitate could be induced during irradiation. Fig. 7 shows a high resolution image and power spectrum obtained from the cascade after electron irradiation to 0.9 dpa at 723 K, where solute concentration changes were identified. Darker contrast with about 16 nm in diameter in Fig. 7(b) is attributed to the segregation. From the power spectrum analysis it was suggested the precipitate corresponds to fcc γ'-Ni_3Si. In austenitic stainless steels containing Si, it has been often observed that the formation of γ' phase (Ni_3Si) in matrix during neutron irradiation at 773 K [18,19]. Therefore it is considered that the precipitates observed in present experiment are the same type.

4. Summary

We have investigated the effect of cascade cluster on precipitation behavior in an austenitic Fe–Cr–Ni alloy containing Si by means of electron irradiation following to ion irradiation. It was observed that two types of defect clusters, namely vacancies and interstitials clusters were introduced around cascade damage region due to Ni^+ ion irradiation at room temperature. The cascades were transferred to SFTs during annealing at 673 K, while dislocation loops were nucleated in the region with interstitials rich zone and grew during electron irradiation at 623 K. When helium were implanted and annealed at 673 K after ion irradiation, He bubbles were formed at cascade. The segregation was also recognized at cascade before and after electron irradiation at 733 K, where Ni and Si concentration increased and Cr was depleted and γ-Ni_3Si precipitates were often formed at the segregated cascade regions. However segregation at the cascade with He could not detected.

References

[1] N.Q. Lam, J. Nucl. Mater. 117 (1983) 106.
[2] G.R. Odette, G.E. Lucas, J. Nucl. Mater. 179–181 (1991) 572.
[3] D.J. Edward, E.P. Simonen, S.M. Bruemmer, J. Nucl. Mater. 317 (2003) 13.
[4] D.J. Bacon, Yu.N. Osetsky, R.E. Stoller, R.E. Voskoboinikov, J. Nucl. Mater. 323 (2003) 152.
[5] M. Kiritani, Point Defects and Defect Interactions in Metals, Yamada Science Foundation, Tokyo University, 1982, p. 59.
[6] B.D. Wirth, V. Bulatov, T. Diaz de la Rubia, J. Nucl. Mater. 283–287 (2000) 773.
[7] R. Schaeublin, M.-J. Caturla, M. Wall, T. Felter, M. Fluss, B.D. Wirth, T. Diaz de la Rubia, M. Victoria, J. Nucl. Mater. 307–311 (2002) 988.
[8] S. Ishino, J. Nucl. Mater. 206 (1993) 139.

[9] R.G. Berggren, J.R. Hawthorne, R.K. Nanstad, Effects of Radiation on Materials, in: F.A. Garner J.S. Perrin (Eds.), 12th International Symposium, ASTM-STM-870, ASTM, 1985, p. 1094.
[10] P.J. Maziasz (Ed.), Effects of Helium Content on Microstructural Development in Type 316 Stainless Steel under Neutron Irradiation, ORNL-6121, 1985.
[11] Y. Hidaka, S. Ohnuki, H. Takahashi, S. Watanabe, J. Nucl. Mater. 212–215 (1994) 330.
[12] R.E. Stoller, G.R. Odette, J. Nucl. Mater. 154 (1988) 1328.
[13] B.N. Singh, S.J. Zinkle, J. Nucl. Mater. 206 (1993) 212.
[14] B.N. Singh, S.I. Golubov, H. Trinkaus, D.J. Edwards, M. Eldrup, J. Nucl. Mater. 328 (2004) 77.
[15] K. Yasuda, T. Yamamoto, M. Shimada, S. Matsumura, Microscopy 41 (2006) 150.
[16] P.R. Okamoto, H. Wiedersich, J. Nucl. Mater. 53 (1974) 336.
[17] T. Takeyama, H. Takahashi, S. Ohnuki, J. Nucl. Mater. 108&109 (1982) 465.
[18] P.J. Maziasz, J. Nucl. Mater. 205 (1993) 118.
[19] I.M. Neklyudov, V.N. Voyevodin, J. Nucl. Mater. 212–215 (1994) 39.